PUFA-Derived *N*-Acylethanolamide Probes Identify Peroxiredoxins and Small GTPases as Molecular Targets in LPS-Stimulated RAW264.7 Macrophages

Ian-Arris de Bus, Antoine H. P. America, Norbert C. A. de Ruijter, Milena Lam, Jasper W. van de Sande, Mieke Poland, Renger F. Witkamp, Han Zuilhof, Michiel G. J. Balvers,* and Bauke Albada*

Read Online

ACCESS | Metrics & More | Article Recommendations | Supporting Information
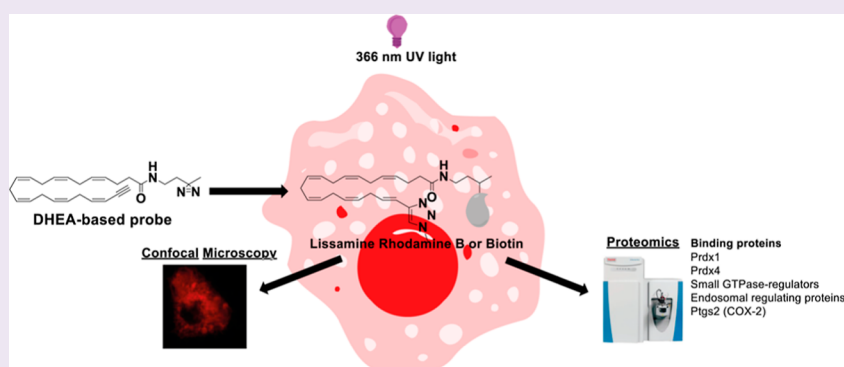
ABSTRACT: We studied the mechanistic and biological origins of anti-inflammatory poly-unsaturated fatty acid-derived *N*-acylethanolamines using synthetic bifunctional chemical probes of docosahexaenoyl ethanolamide (DHEA) and arachidonoyl ethanolamide (AEA) in RAW264.7 macrophages stimulated with 1.0 μg mL^{-1} lipopolysaccharide. Using a photoreactive diazirine, probes were covalently attached to their target proteins, which were further studied by introducing a fluorescent probe or biotin-based affinity purification. Fluorescence confocal microscopy showed DHEA and AEA probes localized in cytosol, specifically in structures that point toward the endoplasmic reticulum and in membrane vesicles. Affinity purification followed by proteomic analysis revealed peroxiredoxin-1 (Prdx1) as the most significant binding interactor of both DHEA and AEA probes. In addition, Prdx4, endosomal related proteins, small GTPase signaling proteins, and prostaglandin synthase 2 (Ptgs2, also known as cyclooxygenase 2 or COX-2) were identified. Lastly, confocal fluorescence microscopy revealed the colocalization of Ptgs2 and Rac1 with DHEA and AEA probes. These data identified new molecular targets suggesting that DHEA and AEA may be involved in reactive oxidation species regulation, cell migration, cytoskeletal remodeling, and endosomal trafficking and support endocytosis as an uptake mechanism.

INTRODUCTION

Poly-unsaturated fatty acids (PUFAs) are essential lipids for human development and functioning, and they support important roles such as immune regulation.[1] Besides PUFAs, their corresponding amides, esters, and ethers also possess immunoregulatory activities.[1−3] Currently, the prototypical endocannabinoid arachidonoyl ethanolamide (AEA, a.k.a. anandamide), the ethanolamine conjugate of arachidonic acid (AA) (20:4*n*-6), has well-described interactions with cannabinoid (CB) and other receptors[1,4−7] and is known to be converted to inflammatory-regulating prostamides.[1,5] Nevertheless, the full spectrum of its uptake and biological mechanisms underlying its effects are not yet fully understood.[1,8] An important structural analogue of AEA is the *n*-3 PUFA amide docosahexaenoyl ethanolamide (DHEA), the ethanolamine conjugate of docosahexaenoic acid (DHA)

(22:6*n*-3). Studies on lipopolysaccharide (LPS)-stimulated mouse-derived RAW264.7 macrophages and microglia cell lines showed that DHEA reduced the formation of nitric oxide (NO), COX-2-derived prostaglandins, and thromboxanes and also lowered expression and production of various inflammatory-regulating cytokines such as monocyte chemoattractant protein-1 (MCP-1), interleukin-6 (IL-6), tumor necrosis factor alpha (TNFα), and IL-1β.[9,10] Apart from cytokine regulation in macrophages, DHEA exerted synaptogenic and neuro-

Figure 1. Schematic application of bifunctional PUFA-derived probes for cellular visualization and proteomic characterization. First, the diazirine group is covalently linked to the molecular (protein) interaction partner(s) when exposed to 366 nm UV irradiation. Then, the PUFA-derived probes are either (i) visualized using CuAAC coupling to a fluorophore or (ii) purified by affinity purification with streptavidin beads and biotinylated probes. Affinity-based purification is followed by tryptic digestion and MS/MS-based characterization. Chemical structures of the natural PUFA derivatives or drugs, and their synthetic derived bifunctional probes, are shown in the figure.

protective effects in neural cells,[10,11] stimulated reactive oxidation species (ROS) production in head and neck squamous cell carcinoma (HNSCC) cells,[12] and reduced inflammatory and nociceptive pain-related behavior in mice.[13] Additionally, DHEA and AEA are metabolized by COX-2, 15-LOX, and CYP450 to yield compounds with distinct anti-inflammatory and antitumorigenic properties.[1,2,14−18] Other studies reported interactions between DHEA and the cannabinoid receptors CB_1/CB_2, transient receptor potential V1 (TRPV-1), and peroxisome proliferator-activated receptors (PPARs), although the obtained agonistic effects seem to depend on the model that was used.[1,9,14,16,19−21] Our previous studies on LPS-stimulated RAW264.7 macrophages did not show DHEA agonism with CB_1/CB_2 or PPARs but rather indicated an important role in reducing COX-2-derived prostaglandins.[9,17] Clearly, many open questions persist about DHEA signaling in LPS-stimulated macrophages.

In the current study, we aim to elucidate underlying mechanisms of the anti-inflammatory effects of AEA and DHEA in 1.0 μg mL^{-1} LPS-stimulated murine RAW264.7 macrophages by applying novel bifunctional PUFA-derived probes (Figure 1). These probes contain a 366 nm UV-active diazirine moiety to covalently attach to their interaction targets and contain a terminal alkyne to selectively purify or visualize the chemical probes using a copper-mediated alkyne−azide click reaction (CuAAC) with biotin or a fluorescent probe, respectively (Figure 1).[1,22,23] Previously, similar methodological setups identified protein interactions with arachidonoyl, oleoyl, palmitoyl, and stearoyl probes in human HEK293T and mouse Neuro2a cells, which led to new druggable sites in the endocannabinoid system.[6] Similarly, nonsteroidal anti-inflammatory drug (NSAID) probes[24] were used to unravel the interaction of celecoxib with prostaglandin E synthase.[25]

Figure 2. Medium concentration of inflammatory regulators released from 1.0 μg mL^{-1} LPS-stimulated RAW264.7 macrophages, incubated with 10 μM DHEA **1**, 10 μM DHEA-derived synthetic probe **2** or **3**, or 10 μM negative control probe **8**. (A) Medium concentrations of PGE$_2$. (B) Medium concentrations of IL-6. Bars represent mean with SD (N = 3, technical duplicates). * indicates significant differences from the vehicle (EtOH) control (one-way ANOVA, Dunnett's multiple comparison post-hoc; *$P < 0.05$, **$P < 0.01$, ***$P < 0.001$). "a" indicates significance between 10 μM DHEA **1** and 10 μM DHEA probe **3** incubation (one-way ANOVA, Tukey's multiple comparison post-hoc; $P < 0.05$).

To characterize new protein interaction partners of DHEA and AEA in LPS-stimulated RAW264.7 macrophages, we first assessed whether our probes displayed comparable biological effects as their parent compounds. Subsequently, we studied their localization in the macrophages by confocal fluorescence microscopy. Affinity purification followed by proteomic analysis enabled analysis of the protein interactome and provided insights into the molecular interaction partners and underlying pathways. Our data confirm previously proposed roles of both AEA and DHEA in the regulation of ROS production, cytoskeletal remodeling, and migration, which we attribute to newly uncovered interactions with peroxiredoxins (Prdxs) and small GTPase signaling proteins.

METHODS

Cell Culture. All cell experiments were performed in RAW264.7 macrophages (American Type Culture Collection) cultured in Dulbecco's modified Eagle's medium (DMEM) containing 10% fetal calf serum (FCS) and 1% penicillin and streptomycin (P/S). Cells were incubated at 37 °C and 5% CO$_2$ in a humidified incubator.

Cytotoxicity and Anti-inflammatory Effects. Macrophages were seeded at 2.5×10^5 cells mL^{-1} and incubated overnight in 24-well plates (Corning Life Sciences) containing 0.5 mL of the medium per well. The medium of adherent cells was discarded and replaced with a fresh medium containing 5 or 10 μM compounds (in 0.1% v/v EtOH for PUFA conjugates or in 0.1% v/v DMSO for indomethacin) or a vehicle (0.1% v/v EtOH or 0.1% v/v DMSO) control. Cells were preincubated with the compounds for 30 min before stimulation with 1.0 μg mL^{-1} LPS in 0.1% phosphate-buffered saline (PBS) or 0.1% PBS control. After LPS addition, cells were incubated for 24 h in the dark (covered with an aluminum foil) to protect the probe from incidental UV exposure. Finally, the medium was collected, and IL-6, PGE$_2$, and LDH concentrations were quantified as described in the Supporting Information.

Proteomic Experiment. In 100 mm culture dishes, RAW264.7 macrophages were seeded at a density of $(0.5-1.0) \times 10^6$ cells mL^{-1} in 15 mL of the medium. After overnight culture, cells were stimulated with 5 mL of the fresh medium containing 1.0 μg mL^{-1} LPS in 0.1% PBS. After 4 h of the LPS stimulation, cells were incubated with 5 mL of the fresh medium containing 1.0 μg mL^{-1} LPS in 0.1% PBS and 10 μM synthetic probes in 0.1% EtOH or DMSO. Probe-treated macrophages were incubated for 4 h in the dark (covered with an aluminum foil). Following incubation, the medium and nonadherent

cells were removed, after which the samples were placed on ice. Illumination with UV light was performed for 10 min at 366 nm and 1 mJ cm^{-2} with an UVP-C1000 crosslinker equipped with five 8 W light bulbs (Supporting Information, Figure 1) or under normal lamp light as control. After light treatment, cells were collected by scraping in 5 mL of the ice cold 1× PBS and used in the proteomic workup (detailed protocol is provided in the Supporting Information).

Fluorescence and Immunostaining. Immunostaining and additional fluorescence click labeling were based on an existing protocol from the study by Gaebler et al.[26] RAW264.7 macrophages were seeded in Ibidi μ-Slide 8-well ibiTreat polymer coverslips (Ibidi GmbH) with a density of 2.5×10^5 cells mL^{-1}, containing 300 μL of the cell suspension per well. Cells were allowed to grow overnight and then prestimulated for 4 h with 1.0 μg mL^{-1} LPS prior to a 4 h incubation with a fresh medium containing 10 μM probe or 0.1% EtOH (vehicle) and 1.0 μg mL^{-1} LPS (LPS prestimulation). Alternatively, cells were directly incubated with 10 μM probes or vehicle together with 1.0 μg mL^{-1} LPS for 4 h (no LPS prestimulation). After incubation, the medium of adherent cells was discarded, and cells were irradiated at 366 nm for 5 min on ice (lamp conditions in probe incubation) or placed on ice under "control" (normal lamp light) conditions. Immunostaining and fluorescence click labeling were performed as described in the Supporting Information.

Statistical Analysis. LDH cytotoxicity, PGE$_2$ ELISA, and IL-6 ELISA samples were measured in three separate experiments containing two technical replicates. Cytotoxicity values were presented as percentages and normalized to 1% Triton X-100 (100% toxicity) and vehicle (0.1% EtOH or DMSO) control (0% toxicity). Cytotoxicity values, PGE$_2$ concentrations, and IL-6 concentrations are presented as mean with the standard deviation (SD). Graphical presentation and statistical analysis using one-way analysis of variance (ANOVA) with Dunnett's multiple comparison post-hoc or Tukey's multiple comparison post-hoc were performed in GraphPad Prism v 5.0.

RESULTS AND DISCUSSION

The bifunctional PUFA amide-derived probes (Figure 1) contain a photo-activatable diazirine for covalent attachment after 366 nm UV light treatment and a terminal alkyne for CuAAC-based affinity purification or labeling with a fluorescent group. Diazirine was introduced at the N-acyl end of PUFA where it likely did not interfere with the
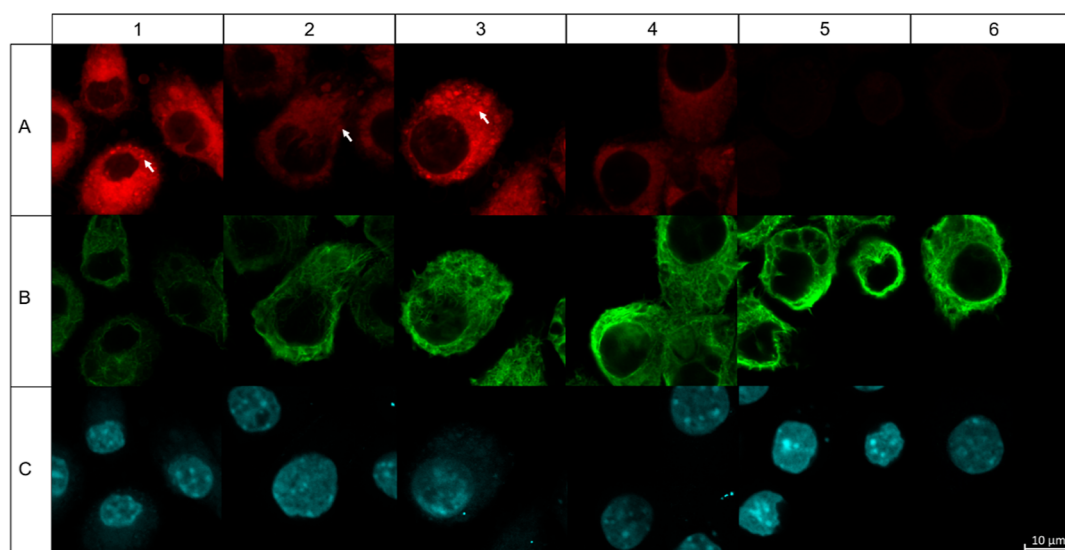
Figure 3. Confocal fluorescent images of 1.0 μg mL^{-1} LPS-stimulated RAW264.7 macrophages. Rows: (A) Lissamine rhodamine B channel after the CuAAC with lissamine rhodamine B. (B) Immunostained tubulin. (C) DAPI staining. Columns: (1) 10 μM DHEA probe **2**. (2) 10 μM DHEA probe **3**. (3) 10 μM AEA probe **5**. (4) 10 μM indomethacin probe **7**. (5) 10 μM probe **8**. (6) 0.1% EtOH vehicle. Arrows highlight vesicle compartmentalization. The scale bar applies to all images in the figure.

biological activity of PUFA-derived amides.[6] Probes **2** and **3** are synthetic derivatives of DHEA **1**, in which probe **2** has alkyne at the *N*-acyl end and probe **3** has alkyne at the PUFA tail. Probe **5** is a synthetic mimic of the *n*-6 PUFA derivative AEA **4**, having alkyne and diazirine at the *N*-acyl end of the molecule; probe **7** is a previously reported NSAID probe of indomethacin **6**[24] and was used as a positive control,[24] and probe **8** is a short pentynoyl-derived negative control probe lacking immunological effects. Identified interactions with control probe **8** are used to filter out nonspecific PUFA-derived probe interactions in the data analysis of the proteomics. Following earlier in vitro studies investigating the anti-inflammatory effect of DHEA and AEA in this and similar models,[9,12,14,15,17,18,21,27] probe concentrations of 10 μM were used, which are of the same order of magnitude or even below those used in comparable studies with similar lipid probes.[6,28,29] Lastly, applying 10 μM probe counters the attrition that is associated with different steps in the methodology (i.e., uptake of probes by macrophages, non-quantitative yield of photolabeling,[22] and loss during enrichment) to obtain sufficient levels of labeled protein above the detection limit of the liquid chromatography tandem mass spectrometry (LC−MS/MS).

Probes Reduce PGE$_2$ and IL-6 Concentrations. We verified that our probes have similar biological effects to their parent compounds by measuring the production of PGE$_2$ and IL-6 as well as the cytotoxicity of the chemical probes in 1.0 μg mL^{-1} LPS-stimulated RAW264.7. No significant cytotoxicity was observed for the PUFA-derived probes, and only for indomethacin probe **7** limited cytotoxicity was observed when compared to the vehicle control (Supporting Information, Figure 2 andTable 2).

Incubation with 10 μM DHEA reduced PGE$_2$ levels in the medium to 89% compared to those in the vehicle control [from 3.62 ± 1.26 ng mL^{-1} to 0.40 ± 0.10 ng mL^{-1} ($P <$ 0.001)], and incubation with 10 μM synthetic DHEA probe **2** or **3** reduced PGE$_2$ levels to 96% [0.16 ± 0.03 ng mL^{-1} ($P <$ 0.001)] or to 93% [0.27 ± 0.05 ng mL^{-1} ($P <$ 0.001)], respectively (Figure 2a and Supporting Information, Table 2).

Similarly, incubation with 10 μM indomethacin or indomethacin probe **7** reduced PGE$_2$ concentrations in the medium to levels below accurately quantifiable concentrations, indicating almost complete inhibition in COX-2 activity (Supporting Information, Table 2). Strong COX-2 inhibition by indomethacin and indomethacin probe **7** was reported previously.[24] Incubation with 10 μM negative control probe **8** resulted in slightly reduced PGE$_2$ levels in the medium (Supporting Information, Table 2).

Similar to those of PGE$_2$, medium IL-6 levels were reduced by DHEA in 1.0 μg mL^{-1} LPS-stimulated macrophages.[9] After 24 h of incubation with 10 μM DHEA, a reduction of 41% in IL-6 medium levels (from 23.7 ± 8.9 to 14.0 ± 5.3 ng mL^{-1}) was observed, not reaching significance. Incubations with 10 μM synthetic DHEA probes **2** and **3** did, however, significantly reduced IL-6 concentrations in the medium to 56% [10.5 ± 3.9 ng mL^{-1} ($P <$ 0.01)] and 68% [7.6 ± 4.3 ng mL^{-1} ($P <$ 0.01)], respectively. Statistical analysis using Tukey's multiple comparison test indicated that incubation with 10 μM DHEA probe **3** was significantly more effective ($P <$ 0.05) in reducing IL-6 production than that with 10 μM DHEA. Control probe **8** (Figure 2b), indomethacin **6**, and indomethacin probe **7** did not significantly affect IL-6 production (Supporting Information, Table 2). IL-6 production was also not significantly affected by AEA or AEA probe **5** when compared to that in vehicle incubation. Remarkably, incubation with 10 μM AEA probe **5** reduced IL-6 levels to 49% (12.2 ± 9.7 ng mL^{-1}), whereas 10 μM AEA increased IL-6 levels to 122% (29.2 ± 10.9 ng mL^{-1}), which corresponds to a significant ($P <$ 0.05) difference between 10 μM AEA and 10 μM AEA probe **5** incubations using Tukey's multiple comparison test (Supporting Information, Table 2). Although this outcome might suggest a distinct immunological effect of AEA and its corresponding probe **5** on IL-6, contradicting literature reports lead us to conclude that IL-6 is probably not a suitable marker for the immunological effects of AEA.[30−32]

In conclusion, we showed that the synthesized DHEA and indomethacin probes mimic the expected anti-inflammatory effects of the parent compounds in 1.0 μg mL^{-1} LPS-
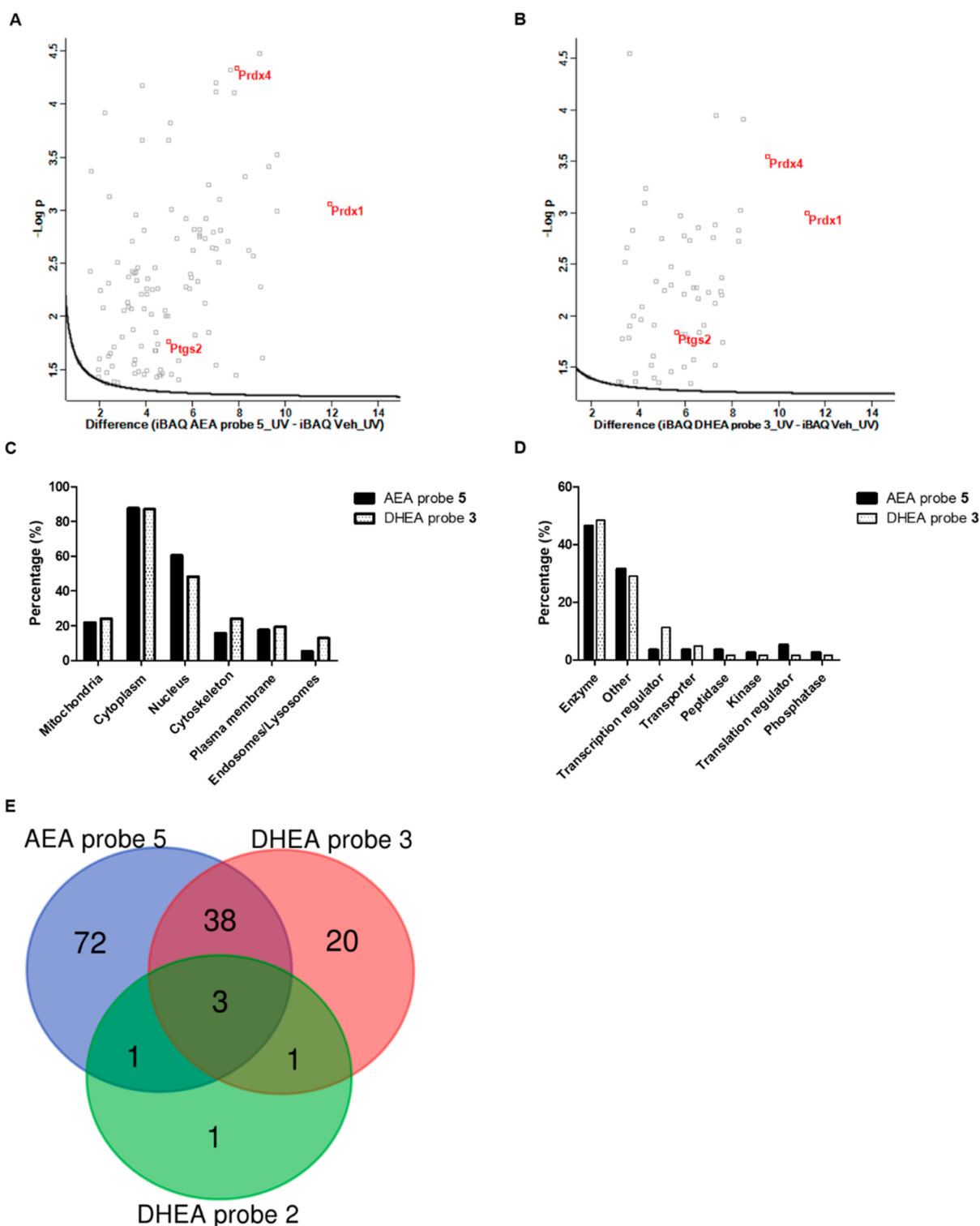
Figure 4. Proteomics analyses of DHEA probes **2** and **3** and AEA probe **5** ($N = 3$). (A) Volcano plot (FDR 0.05, S0 0.1) of AEA probe **5**. (B) Volcano plot (FDR 0.05, S0 0.1) of DHEA probe **3**. Both (A) and (B) show sequentially filtered data against the vehicle (0.1% EtOH control). *X*-axis represents 2log[iBAQ] value (probe−vehicle) differences, and *y*-axis represents −log *p* values. (C) Protein ontology of AEA probe **5** and DHEA probe **3** targets according to UniProt. (D) Cellular function of AEA probe **5** and DHEA probe **3** targets according to IPA. (E) Venn diagram of DHEA probes **2** and **3** and AEA probe **5** targets.

stimulated RAW264.7 macrophages, which was not the case for our negative control probe **8**.

Synthetic Probes Localize around the ER and in Membrane Vesicles. To better understand the biological functionality of our compounds, we first analyzed the in vitro

localization of 4 h incubated 10 μM synthetic probes in 1.0 μg mL^{-1} LPS-stimulated RAW264.7 macrophages. The probes were visualized with lissamine rhodamine B PEG3 azide using tetrakis(acetonitrile)copper(I) hexafluorophosphate in chemically fixed cells that were immunostained with alpha-tubulin

Table 1. Protein Targets of DHEA Probe 3 (Top) and AEA Probe 5 (Bottom)[a]

Protein IDs	Protein names	Gene names	-Log Student's T-test p-value iBAQ DHEA probe 3 vs. iBAQ Vehicle (0.1% EtOH)	Student's T-test Difference iBAQ DHEA probe 3 vs. iBAQ Vehicle (0.1% EtOH)
P35700	Peroxiredoxin-1	Prdx1	2.99	11.2
O08807	Peroxiredoxin-4	Prdx4	3.54	9.52
P47911	60S ribosomal protein L6	Rpl6	3.91	8.47
Q60605; Q8CI43	Myosin light polypeptide 6	Myl6	3.02	8.38
P47738	Aldehyde dehydrogenase, mitochondrial	Aldh2	2.72	8.30
P62821; Q9D1G1	Ras-related protein Rab-1A;Ras-related protein Rab-1B	Rab1A;Rab1b	2.83	8.28
P35278	Ras-related protein Rab-5C	Rab5c	1.74	7.63
P50580	Proliferation-associated protein 2G4	Pa2g4	2.20	7.59
P45376	Aldose reductase	Akr1b1	2.37	7.56
Q64282	Interferon-induced protein with tetratricopeptide repeats 1	Ifit1	2.24	7.55
Protein IDs	**Protein names**	**Gene names**	**-Log Student's T-test p-value iBAQ AEA probe 5 vs. iBAQ Vehicle (0.1% EtOH)**	**Student's T-test Difference iBAQ AEA probe 5 vs. iBAQ Vehicle (0.1% EtOH)**
P35700	Peroxiredoxin-1	Prdx1	3.06	11.9
Q9JJI8	60S ribosomal protein L38	Rpl38	3.52	9.64
Q62159; P62746	Rho-related GTP-binding protein RhoC	Rhoc	2.99	9.64
Q9Z1N5	Spliceosome RNA helicase Ddx39b	Ddx39b	3.41	9.31
Q8BFZ3	Beta-actin-like protein 2	Actbl2	1.61	9.02
P47915	60S ribosomal protein L29	Rpl29	2.28	8.94
P62245	40S ribosomal protein S15a	Rps15a	4.47	8.90
Q8BP67	60S ribosomal protein L24	Rpl24	2.57	8.63
O09167	60S ribosomal protein L21	Rpl21	2.62	8.42
Q8QZT1	Acetyl-CoA acetyltransferase, mitochondrial	Acat1	3.31	8.27

[a]Top 10 protein differences between vehicle (0.1% EtOH) and 10 μM probes. Protein differences [2log[iBAQ] values (probe−vehicle)] and p-values were determined using a two-sample Student's t-test ($p < 0.05$).

AlexaFluor488 and nuclear 4′,6-diamidino-2-phenylindole (DAPI) dsDNA staining (Figure 3). Control samples showed no nonspecific labeling of lissamine rhodamine B and AlexaFluor 488 (Supporting Information, Figures 3 and 4).

DHEA probe **2** was taken up by LPS-stimulated RAW264.7 macrophages in 4 h and localized around the nuclear periphery in cytosol, suggesting agglomeration in the endoplasmic reticulum (ER) and golgi system (Figure 3-1A). In addition, DHEA probe **2** clustered in spherical membrane domains. As the slightly different DHEA probe **3** showed similar intracellular localization to that of DHEA probe **2** (Figure 3-2A), we conclude that the observations relate to the localization of intact DHEA probes. Similarly, AEA probe **5** showed cytoplasmatic staining and an apparent high level of spherical domain compartmentalization (Figure 3-3A). Therefore, PUFA-derived amides tend to localize around the ER where they are generally catabolized by enzymes like COX-2.[33] To show that the N-acylethanolamide probes are not extensively metabolized within cultured cells, additional metabolic tracing experiments using TLC fluorescence were performed (Sup-

porting Information, Figure 5), applying a similar approach to that reported in the study by Thiele and co-workers.[34] This experiment indicated that the parent DHEA probe 3 remained largely intact after incubation for 4 h with 1.0 μg/mL LPS-stimulated RAW264.7 macrophages, apart from a minor metabolite with slightly increased hydrophilicity as shown by a lower R_f value. Based on our previous observations, we hypothesize that this product most likely represents hydroxylated metabolites of the DHEA probe at the 13- and 16-position, which have been characterized as metabolites in this model.[17] Together, these findings indicate that the intact probe remains available under the study conditions used. This is in line with previous results where we showed that intracellular DHEA concentrations in LPS-stimulated RAW264.7 macrophages remained stable for 48 h[17] and that incubation with DHEA did not lead to measurable DHA levels in the medium of LPS-stimulated RAW264.7 macrophages.[9]

Indomethacin probe **7** labeling was weaker than that with PUFA derivatives and was also localized inside the cytoplasm (Figure 3-4A). For control probe **8**, we observed almost no

fluorescence labeling, suggesting its limited uptake or rapid breakdown (Figure 3-5A). Control incubations with the vehicle (0.1% EtOH) showed no background fluorescence from lissamine rhodamine B (Figure 3-6A).

The specific counterstaining of alpha-tubulin resulted in an AlexaFluor 488-stained cytoskeleton (Figure 3B), proving that fixation and immunofluorescence are successfully combined with click labeling of lipids, as reported previously.[26] Z-stack projection of tubulin staining additionally showed fine tubulin structures indicating no or limited fixation damage during the preparation of the slides (Supporting Information, Figure 6 and Video S1). DAPI staining of nuclei clearly showed more intense labeling of condensed heterochromatic segments and less intense signals of euchromatic segments in the nucleus (Figure 3C). Our confocal fluorescence analysis provided evidence for the uptake of our PUFA probes 2 and 3 as well as indomethacin probe 7 in LPS-stimulated macrophages over a period of 4 h, resulting in localization around the ER and in membrane vesicles.

Characterization of the PUFA-Derived Probe Interactome. Molecular interaction partners of our probes were identified by proteomic characterization of the interactome in 8 h LPS-stimulated and 4 h probe-incubated macrophages. Data analysis using iBAQ scores enabled identification of relative abundances of proteins.[35,36] After filtering out nonspecific background interactions using signals from the vehicle (0.1% EtOH) incubations and statistical evaluation using a two-sample Student's t-test ($p < 0.05$ and t-test difference > 1.0), 101 significantly enriched proteins were found for DHEA probe 2, 198 proteins for DHEA probe 3, 273 proteins for AEA probe 5, and 55 proteins for indomethacin probe 7. Sequential filtering using the randomly interacting control probe 8 and a second two-sample Student's t-test ($p < 0.05$ and t-test difference > 1.0) resulted in 6 significantly enriched proteins for DHEA probe 2, 62 proteins for DHEA probe 3, 114 proteins for AEA probe 5, and 4 proteins for indomethacin probe 7. Significantly enriched proteins resulting from the sequential filtering were displayed against the vehicle (0.1% EtOH) treatment (Figure 4A,B and Supporting Information, Table 3). Despite sequential filtering, also with probe 8, we identified targets such as ribosomal and cytoskeletal proteins, which are likely nonspecific, highly abundant protein targets that are often observed in similar affinity-based proteomic setups.[6,24,28] Notwithstanding, comparison of enriched proteins with previous chemical proteomic enrichment studies revealed that 52 of the 114 AEA probe 5 targets were also enriched by A-DA and/or AEA-DA, two AEA-based chemical probes, in HEK293T/Neuro2a cells.[6] Moreover, DHEA probe 3 and AEA probe 5 were found to interact with prostaglandin synthase 2 (Ptgs2; also known as COX-2); we and others previously demonstrated that this enzyme is involved in the oxygenation of AEA and DHEA (Figure 4A,B).[5,17] These data support that our used methodology, comprising stringent washing of the affinity-labeled proteins with 3 × 3 washing steps, including a strong wash with 4 M urea and 0.4% SDS in ice cold 1× PBS containing a 1× cOmplete protease inhibitor, and sequential data filtering with a nonspecific binding control probe 8, leads to detection of expected binding targets.

UniProt database and ingenuity pathway analysis (IPA) were used to identify cellular domain(s) and functional annotation of the protein targets (Figure 4C,D). Most proteins are localized in the cytoplasm (Figure 4C), confirming our observed cytoplasmatic localization (Figure 3). In addition to enzymes, we identified transcription and translation regulators, as well as transporters (Figure 4D). Comparison of the enriched proteins for DHEA probes 2 and 3 and AEA probe 5 revealed that only three proteins interacted with all three PUFA amide probes (Figure 4E). In total, 38 shared targets were found for DHEA probe 3 and AEA probe 5, whereas 20 proteins were specific targets of DHEA probe 3, and 72 proteins were specific targets of AEA probe 5.

Both DHEA probe 3 and AEA probe 5 showed the strongest specific interaction with Prdx 1 (Prdx1) (Figure 4A,B and Table 1). Also, Prdx4 labeling was significant for both PUFA-derived amide probes (Figure 4A,B). Prdxs convert hydrogen peroxide to water and lipid hydroperoxides to alcohols, protecting the cells from ROS toxicity.[37,38] Although many studies described the anti-inflammatory and protective effects of Prdxs, Prdx1 knockdown decreased inflammatory cytokine production and increased anti-inflammatory IL-10 production in LPS-stimulated RAW264.7 macrophages.[39] The selective binding of our PUFA amides to Prdx1 could therefore be linked with the blockage of the Prdx1-induced inflammation in RAW264.7 cells. Previous proteomic screening with AA, the PUFA precursor of AEA, also showed an interaction of AA with ROS regulators in RAW264.7 macrophages, which was ascribed to the induction of lipid electrophile-driven coupling upon stimulation of the macrophages with the LPS mimetic Kdo_2-lipid A.[29] Although our methodology used diazirine crosslinking, lipid electrophile coupling to ROS scavengers could not be ruled out as a possible interaction mechanism between AEA, DHEA, and Prdxs. Interestingly, both DHEA and AEA were reported to induce the ROS production in HNSCC cells,[12,27] and in 0.1 μg mL^{-1} LPS-stimulated mouse macrophages, 10 nM DHEA was found to reduce ROS production.[10] In addition to Prdxs, we found ribosomal proteins, acetyl-CoA acetyltransferase (Acat1, mitochondrial), and the signaling regulator Rhoc in the top 10 AEA probe 5 interactors (Table 1).[40]

The top 10 DHEA probe 3 interactors showed two intracellular membrane trafficking proteins: Rab1a and Rab5c (Table 1). Rab1a regulates cell adhesion and cell migration via β1 integrin recycling and is localized in the ER and intracellular vesicle domains where DHEA was localized (Figure 3).[41] Rab5c is a key regulator in early endosome trafficking and is involved in cell migration via β1 integrin recycling.[42] Interestingly, these observations add to the ongoing debate concerning the uptake mechanism of PUFA derivatives, occurring via a currently unidentified membrane transporter or via passive diffusion.[8,43] Characterization of endosomal proteins interacting with DHEA probe 3 and AEA probe 5 might indicate that lipid raft- and caveolae-dependent endocytosis is an uptake route for those PUFA-derivatives, as was previously suggested for AEA in the study by McFarland and co-workers.[44] This hypothesis is further supported by the identification of the DHEA probe 3 interactor Dnm2, which has important functions in endosomal formation (Supporting Information, Table 3).[45] Clearly, focused studies should be aimed at unraveling the uptake mechanisms of AEA and DHEA to support an endocytosis-dependent uptake mechanism. The transcription regulator Pa2g4 and the pro-inflammatory immune regulator Ifit1 were also significantly bound by DHEA probe 3. Recently, we reported that the expression of Ifit1 was reduced as a result of incubation with 5 μM 13-HDHEA and 16-HDHEA (hydroxydocosahexaenoyl
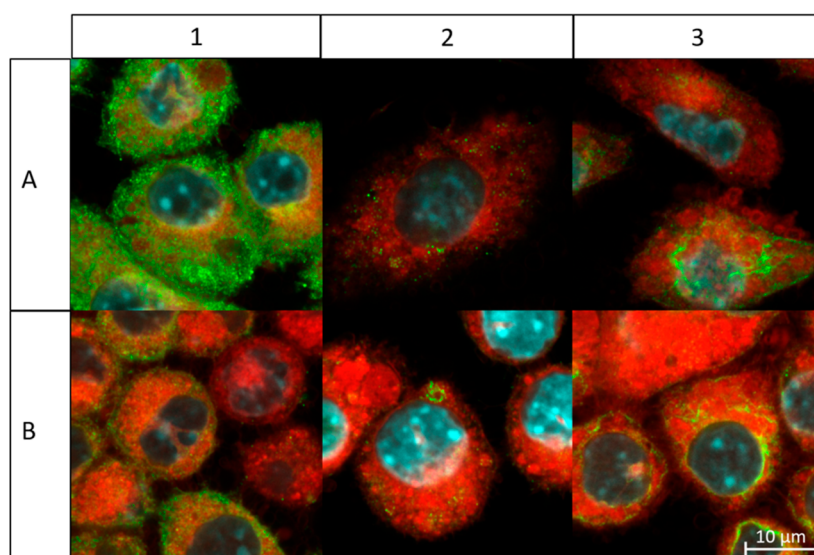
Figure 5. Confocal fluorescent images of probe-incubated RAW264.7 macrophages prestimulated for 4 h with 1.0 μg mL^{-1} LPS. (A) Cells incubated with fresh 1.0 μg mL^{-1} LPS and 10 μM DHEA probe **3** for an additional 4 h. (B) Cells incubated with fresh 1.0 μg mL^{-1} and 10 μM AEA probe **5** for an additional 4 h. Color overlays represent lissamine rhodamine B (red), AlexaFluor 488 antibody (green), and DAPI staining (blue). (1) Rac1 labeling, (2) Rab5c labeling, and (3) Ptgs2 labeling. The scale bar applies to all images in the figure.

ethanolamide), products of the interaction between DHEA and COX-2.[18] As a significant Ifit1 interaction with AEA probe **5** was not observed here, it appears that Ifit1 is only involved in the signaling of DHEA or its metabolites. Interestingly, previously described endocannabinoid-interacting proteins, for example, CB1, CB2, and GPR55, as well as TRPV1 and PPAR,[1,3,4,7,8,19,21] are not identified in our model, likely due to poor expression of those proteins in LPS-stimulated RAW264.7 macrophages.[9]

In conclusion, we observed Prdx-1, Prdx-4, Rhoc, and Acat1 as important AEA probe interactors in LPS-stimulated RAW264.7 macrophages. From these targets, only Prdx-1 was already characterized as a potential AEA target.[6] In addition to these AEA targets, Prdx1, Rab1a, Rab5c, Pa2g4, and Ifit1 were identified as most important DHEA-interacting proteins. Our chemical biological high-throughput method enabled the identification of novel PUFA-amide targets that could not have been revealed with classical endocannabinoid receptor binding studies.

IPA Indicates the Involvement of GTPase Signaling. Functional IPA revealed that enriched protein targets of DHEA probe **3** and AEA probe **5** are mainly involved in Rho family GTPase signaling and actin regulation (Supporting Information, Table 4). A notable protein in the regulation of this pathway is Rac1, which was identified as a significant interactor with DHEA probe **3** and AEA probe **5** but did suffer from relatively weak spectral matching scores and should, therefore, be interpreted with care. Notwithstanding, 21 of the 62 protein hits from DHEA probe **3** and 48 of the 114 protein hits from AEA probe **5** (including Rac1 itself) were identified as (putative) Rac1-interacting proteins to further support the potential role of Rac1 in PUFA-derived amide-mediated GTPase signaling.[46,47] Rho GTPase signaling plays an important role in ROS signaling, cell migration, cytoskeletal remodeling, and actin regulation.[47−49] Indeed, these phenotypic effects can be related to previously reported functions of DHEA and AEA. The effects of DHEA and AEA on ROS regulation were already described above, and other studies have reported antimigratory properties of AEA[3,4,10] and

DHEA,[10] including its oxidized metabolites.[15,16,18] In addition to small GTPase signaling, several actin and myosin-related proteins were also significantly affected by DHEA probe **3** and AEA probe **5**, suggesting that cytoskeletal remodeling is a prerequisite for migration.

Disease and function analysis in IPA showed indications of a response similar to that for viral infections for DHEA probe **3** proteins and cellular organization, response to viral infections, and reduced cell death for AEA probe **5** proteins. However, as IPA uses experimental results from literature reports, it is suboptimal for our current methodology, which was aimed at unraveling novel interactions. In conclusion, links to ROS signaling, actin remodeling, and cell migration were obtained using IPA, but additional research is required to prove that these effects are mediated by GTPase signaling via DHEA and AEA interactions.

Colocalization Supports DHEA and AEA Interactions with Rac1 and Ptgs2. To support a suggested role in endosomal trafficking, Rho GTPase signaling, and lipid metabolism, we performed fluorescence confocal imaging studies staining DHEA probe **3** and AEA probe **5** with lissamine rhodamine B and Rab5c, Rac1, and Ptgs2 with AlexaFluor488 immunostaining (Figure 5). RAW264.7 macrophages were prestimulated for 4 h with 1.0 μg mL^{-1} LPS and subsequently exposed to 10 μM DHEA probe **3** or 10 μM AEA probe **5** and 1.0 μg mL^{-1} LPS for 4 h, mimicking conditions of the proteomic experiment to allow correlations. In addition to midplane images (Figure 5), Z-stack series were recorded, showing that midplane images are representative for the fluorescence localization (Videos S2, S3, S4, S5, S6, and S7). Cytoplasmatic localization was observed for the green Rac1 channel that often colocalized with the spectrally well-separated red PUFA-derived probes in the cell (Figure 5-1A,B), indicating the potential interaction of Rac1 with the PUFA probes. Nonetheless, areas that contained only a signal corresponding to Rac1 or to the PUFA-derived probes were also obtained. Rab5c immunostaining resulted in localization of small vesicles, possibly representing late endosomes, but showed no clear colocalization with our probes (Figure 5-

2A,B). Ptgs2 staining showed main Ptgs2 signals at the cytoplasmic face of the nuclear periphery, known to be rich in the ER where Ptgs2 synthesis takes place (Figure 5-3A,B).[50] Interestingly, the fluorescence signal of the PUFA amide probes was also relatively strong in the nuclear periphery. Although areas of colocalizing Ptgs2- and PUFA-derived amide probes were observed, the signal from Ptgs2 and the probes did not fully colocalize. Even though colocalization within the same voxel (∼270 × 270 × 1000 nm) does not directly prove a molecular interaction, this is a prerequisite. Nevertheless, our observations further support that PUFA-derived amides could interact with multiple partners including Rac1 and Ptgs2. Direct proof for the interaction between the PUFA amides and Ptgs2 was indeed previously demonstrated by the Ptgs2-mediated catabolic conversion of AEA and DHEA.[1,5,17] Controls without primary Rac1, Rab5c, and Ptgs2 antibodies showed no immunofluorescence, indicating specificity of the antibodies and immunostaining protocol (Supporting Information, Figure 6). In conclusion, confocal fluorescence microscopy showed colocalization between the PUFA-derived probes and Rac1 and Ptgs2 as a prerequisite for a molecular interaction. Together with the previously characterized biochemical interaction in the proteomic setup and the reported metabolic interaction between the PUFA amides and Ptgs2, these data strongly support a functional interaction.

CONCLUSIONS

Chemical probes of DHEA and AEA containing two specific tagging functionalities showed that PUFA amides interact with Prdx1, Prdx4, endosomal proteins such as Rab1 and Rab5c, and proteins of the GTPase-signaling pathway in LPS-stimulated RAW264.7 macrophages, rather than only with Ptgs2. In addition, fluorescence labeling of our probes indicated localization in the cytosol, and seemingly the ER and Golgi system, next to compartmentalization in membrane vesicles. Colocalization experiments using confocal fluorescence microscopy supported interactions between PUFA-derived probes and the small GTPase-regulating protein Rac1 as well as Ptgs2. Together, these observations provide novel insights into cellular PUFA amide interactions and their effects on cytoskeletal remodeling, cell migration, and ROS regulation. In addition, our results provide evidence for passive endosomal uptake mediated by lipid rafts.

In view of the unnaturally high lipid probe concentrations used in our and similar in vitro studies, future research should strengthen the interactome data sets by further research on the biological relevance of the identified proteins targets. Additional details regarding PUFA amide−protein interactions that regulate ROS formation, cytoskeletal remodeling, and cell migration may be obtained, as well as support of a lipid raft-dependent uptake mechanism of PUFA-derived amides. This might enable translation of the in vitro effects of DHEA and AEA to in vivo models and ultimately to human metabolism.

ASSOCIATED CONTENT

Ⓢ Supporting Information

The Supporting Information is available free of charge at https://pubs.acs.org/doi/10.1021/acschembio.1c00355.

Summary of all significant protein hits per probe (XLSX)

Overview of the IPA pathways involved for the probe-targeting proteins (XLSX)

Z-stack of the confocal fluorescent images of RAW264.7 macrophages stained with Indomethacin probe 7 and Tubulin (AVI)

Z-stack of the confocal fluorescent images of RAW264.7 macrophages stained with DHEA probe 3 and Rac1 (AVI)

Z-stack of the confocal fluorescent images of RAW264.7 macrophages stained with DHEA probe 3 and Rab5c (AVI)

Z-stack of the confocal fluorescent images of RAW264.7 macrophages stained with DHEA probe 3 and Ptgs2 (AVI)

Z-stack of the confocal fluorescent images of RAW264.7 macrophages stained with AEA probe 5 and Rac1 (AVI)

Z-stack of the confocal fluorescent images of RAW264.7 macrophages stained with AEA probe 5 and Rab5c (AVI)

Z-stack of the confocal fluorescent images of RAW264.7 macrophages stained with AEA probe 5 and Ptgs2 (AVI)

Cytotoxicity, prostaglandin, and cytokine release in probe-incubated RAW264.7 macrophages; control experiments for the confocal fluorescence microscopy; fluorescent TLC experiment to prove the cellular stability of DHEA probe 3; and extended methodology section including synthesis, purification, characterization, and quantification of the chemical PUFA-derived amide probes (PDF)

AUTHOR INFORMATION

Corresponding Authors

Michiel G. J. Balvers − *Division of Human Nutrition and Health, Wageningen University & Research, 6708 WE Wageningen, The Netherlands*; Email: michiel.balvers@wur.nl

Bauke Albada − *Laboratory of Organic Chemistry, Wageningen University & Research, 6708 WE Wageningen, The Netherlands*; ⓞ orcid.org/0000-0003-3659-2434; Email: bauke.albada@wur.nl

Authors

Ian-Arris de Bus − *Division of Human Nutrition and Health, Wageningen University & Research, 6708 WE Wageningen, The Netherlands; Laboratory of Organic Chemistry, Wageningen University & Research, 6708 WE Wageningen, The Netherlands;* ⓞ orcid.org/0000-0002-1061-8352

Antoine H. P. America − *Wageningen Plant Research, Business Unit Bioscience, Wageningen University & Research, 6708 PB Wageningen, The Netherlands*

Norbert C. A. de Ruijter − *Laboratory of Cell Biology, Wageningen Light Microscopy Centre, Wageningen University & Research, 6708 PB Wageningen, The Netherlands*

Milena Lam − *Laboratory of Organic Chemistry, Wageningen University & Research, 6708 WE Wageningen, The Netherlands;* ⓞ orcid.org/0000-0002-8106-0309

Jasper W. van de Sande − *Laboratory of Organic Chemistry, Wageningen University & Research, 6708 WE Wageningen, The Netherlands;* ⓞ orcid.org/0000-0002-4483-5056

Mieke Poland − *Division of Human Nutrition and Health, Wageningen University & Research, 6708 WE Wageningen, The Netherlands*

Renger F. Witkamp − *Division of Human Nutrition and Health, Wageningen University & Research, 6708 WE Wageningen, The Netherlands*

Han Zuilhof − *Laboratory of Organic Chemistry, Wageningen University & Research, 6708 WE Wageningen, The Netherlands; School of Pharmaceutical Sciences and Technology, Tianjin University, 300072 Tianjin, People's Republic of China; Department of Chemical and Materials Engineering, Faculty of Engineering, King Abdulaziz University, 21589 Jeddah, Saudi Arabia;* ◉ orcid.org/0000-0001-5773-8506

Complete contact information is available at:
https://pubs.acs.org/10.1021/acschembio.1c00355

Author Contributions

M.G.J.B. and B.A. contributed equally to this manuscript. The research study was conceived by I.d.B., R.W., H.Z., M.B., and B.A. I.d.B. performed most experiments; M.L. helped with the synthesis of the chemical probes; J.S. performed the TLC experiments; and M.P. assisted with the cell culturing and incubations for the TLC experiments and proteomics. T.A. performed the proteomics LC−MS analysis and assisted with proteomic data analysis; N.d.R. assisted with the fluorescence microscopy measurement, data interpretation, and optimization of the immunostaining protocol. All authors contributed and agreed to the paper.

Notes

The authors declare no competing financial interest.

■ REFERENCES

(1) de Bus, I.; Witkamp, R.; Zuilhof, H.; Albada, B.; Balvers, M. The role of n-3 PUFA-derived fatty acid derivatives and their oxygenated metabolites in the modulation of inflammation. *Prostag. Other Lipid Mediat.* **2019**, *144*, 106351.

(2) Watson, J. E.; Kim, J. S.; Das, A. Emerging class of omega-3 fatty acid endocannabinoids & their derivatives. *Prostag. Other Lipid Mediat.* **2019**, *143*, 106337.

(3) Chiurchiù, V.; Battistini, L.; Maccarone, M. Endocannabinoid signalling in innate and adaptive immunity. *Immunology* **2015**, *144*, 352−364.

(4) Turcotte, C.; Chouinard, F.; Lefebvre, J. S.; Flamand, N. Regulation of inflammation by cannabinoids, the endocannabinoids 2-arachidonoyl-glycerol and arachidonoyl-ethanolamide, and their metabolites. *J. Leukoc. Biol.* **2015**, *97*, 1049−1070.

(5) Alhouayek, M.; Muccioli, G. G. COX-2-derived endocannabinoid metabolites as novel inflammatory mediators. *Trends Pharmacol.* **2014**, *35*, 284−292.

(6) Niphakis, M. J.; Lum, K. M.; Cognetta, A. B.; Correia, B. E.; Ichu, T.-A.; Olucha, J.; Brown, S. J.; Kundu, S.; Piscitelli, F.; et al. A Global Map of Lipid-Binding Proteins and Their Ligandability in Cells. *Cell* **2015**, *161*, 1668−1680.

(7) Pertwee, R. G.; Howlett, A. C.; Abood, M. E.; Alexander, S. P. H.; Di Marzo, V.; Elphick, M. R.; Greasley, P. J.; Hansen, H. S.; Kunos, G.; Mackie, K.; et al. International Union of Basic and Clinical Pharmacology. LXXIX. Cannabinoid Receptors and Their Ligands: Beyond CB1 and CB2. *Pharmacol. Rev.* **2010**, *62*, 588−631.

(8) Maccarone, M. Metabolism of the Endocannabinoid Anandamide: Open Questions after 25 Years. *Front. Mol. Neurosci.* **2017**, *10*, 166.

(9) Meijerink, J.; Poland, M.; Balvers, M. G. J.; Plastina, P.; Lute, C.; Dwarkasing, J.; van Norren, K.; Witkamp, R. F. Inhibition of COX-2-mediated eicosanoid production plays a major role in the anti-inflammatory effects of the endocannabinoid N-docosahexaenoyle-thanolamine (DHEA) in macrophages. *Br. J. Pharmacol.* **2015**, *172*, 24−37.

(10) Park, T.; Chen, H.; Kim, H.-Y. GPR110 (ADGRF1) mediates anti-inflammatory effects of N-docosahexaenoylethanolamine. *J. Neuroinflammation* **2019**, *16*, 225.

(11) Lee, J.-W.; Huang, B. X.; Kwon, H.; Rashid, M. A.; Kharebava, G.; Desai, A.; Patnaik, S.; Marugan, J.; Kim, H.-Y. Orphan GPR110 (ADGRF1) targeted by N-docosahexaenoylethanolamine in development of neurons and cognitive function. *Nat. Commun.* **2016**, *7*, 13123.

(12) Park, S.-W.; Hah, J. H.; Oh, S.-M.; Jeong, W.-J.; Sung, M.-W. 5-lipoxygenase mediates docosahexaenoyl ethanolamide and N-arachidonoyl-L-alanine-induced reactive oxygen species production and inhibition of proliferation of head and neck squamous cell carcinoma cells. *BMC Cancer* **2016**, *16*, 458.

(13) Paton, K. F.; Shirazi, R.; Vyssotski, M.; Kivell, B. M. N-docosahexaenoyl ethanolamine (synaptamide) has antinociceptive effects in male mice. *Eur. J. Pain* **2020**, *24*, 1990−1998.

(14) McDougle, D. R.; Watson, J. E.; Abdeen, A. A.; Adili, R.; Caputo, M. P.; Krapf, J. E.; Johnson, R. W.; Kilian, K. A.; Holinstat, M.; Das, A. Anti-inflammatory ω-3 endocannabinoid epoxides. *Proc. Natl. Acad. Sci. U.S.A.* **2017**, *114*, E6034−E6043.

(15) Roy, J.; Watson, J. E.; Hong, I. S.; Fan, T. M.; Das, A. Antitumorigenic Properties of Omega-3 Endocannabinoid Epoxides. *J. Med. Chem.* **2018**, *61*, 5569−5579.

(16) Yang, R.; Fredman, G.; Krishnamoorthy, S.; Agrawal, N.; Irimia, D.; Piomelli, D.; Serhan, C. N. Decoding Functional Metabolomics with Docosahexaenoyl Ethanolamide (DHEA) Identifies Novel Bioactive Signals. *J. Biol. Chem.* **2011**, *286*, 31532−31541.

(17) de Bus, I.; Zuilhof, H.; Witkamp, R.; Balvers, M.; Albada, B. Novel COX-2 products of n-3 polyunsaturated fatty acid-ethanolamine-conjugates identified in RAW 264.7 macrophages. *J. Lipid Res.* **2019**, *60*, 1829−1840.

(18) de Bus, I.; van Krimpen, S.; Hooiveld, G. J.; Boekschoten, M. V.; Poland, M.; Witkamp, R. F.; Albada, B.; Balvers, M. G. J. Immunomodulating effects of 13- and 16-hydroxylated docosahexaenoyl ethanolamide in LPS stimulated RAW264.7 macrophages. *Biochim. Biophys. Acta Mol. Cell Biol. Lipids* **2021**, *1866*, 158908.

(19) Alharthi, N.; Christensen, P.; Hourani, W.; Ortori, C.; Barrett, D. A.; Bennett, A. J.; Chapman, V.; Alexander, S. P. H. n−3 polyunsaturated N-acylethanolamines are CB2 cannabinoid receptor-preferring endocannabinoids. *Biochim. Biophys. Acta Mol. Cell Biol. Lipids* **2018**, *1863*, 1433−1440.

(20) Brown, I.; Lee, J.; Sneddon, A. A.; Cascio, M. G.; Pertwee, R. G.; Wahle, K. W. J.; Rotondo, D.; Heys, S. D. Anticancer effects of n-3 EPA and DHA and their endocannabinoid derivatives on breast cancer cell growth and invasion. *Prostagl. Leukot. Essent. Fat. Acids* **2020**, *156*, 102024.

(21) Rovito, D.; Giordano, C.; Vizza, D.; Plastina, P.; Barone, I.; Casaburi, I.; Lanzino, M.; De Amicis, F.; Sisci, D.; Mauro, L.; et al. Omega-3 PUFA ethanolamides DHEA and EPEA induce autophagy through PPARγ activation in MCF-7 breast cancer cells. *J. Cell. Physiol.* **2013**, *228*, 1314−1322.

(22) Dubinsky, L.; Krom, B. P.; Meijler, M. M. Diazirine based photoaffinity labeling. *Bioorg. Med. Chem.* **2012**, *20*, 554−570.

(23) Wright, M. H.; Sieber, S. A. Chemical proteomics approaches for identifying the cellular targets of natural products. *Nat. Prod. Rep.* **2016**, *33*, 681−708.

(24) Gao, J.; Mfuh, A.; Amako, Y.; Woo, C. M. Small Molecule Interactome Mapping by Photoaffinity Labeling Reveals Binding Site Hotspots for the NSAIDs. *J. Am. Chem. Soc.* **2018**, *140*, 4259−4268.

(25) Miyamoto, D. K.; Flaxman, H. A.; Wu, H.-Y.; Gao, J.; Woo, C. M. Discovery of a Celecoxib Binding Site on Prostaglandin E Synthase (PTGES) with a Cleavable Chelation-Assisted Biotin Probe. *ACS Chem. Biol.* **2019**, *14*, 2527−2532.

(26) Gaebler, A.; Penno, A.; Kuerschner, L.; Thiele, C. A highly sensitive protocol for microscopy of alkyne lipids and fluorescently tagged or immunostained proteins. *J. Lipid Res.* **2016**, *57*, 1934−1947.

(27) Park, S.-W.; Kim, J.-E.; Oh, S.-M.; Cha, W.-J.; Hah, J.-H.; Sung, M.-W. Anticancer effects of anandamide on head and neck squamous cell carcinoma cells via the production of receptor-independent reactive oxygen species. *Head Neck* **2015**, *37*, 1187−1192.

(28) Isobe, Y.; Kawashima, Y.; Ishihara, T.; Watanabe, K.; Ohara, O.; Arita, M. Identification of Protein Targets of 12/15-Lipoxygenase-Derived Lipid Electrophiles in Mouse Peritoneal Macrophages Using Omega-Alkynyl Fatty Acid. *ACS Chem. Biol.* **2018**, *13*, 887−893.

(29) Beavers, W. N.; Rose, K. L.; Galligan, J. J.; Mitchener, M. M.; Rouzer, C. A.; Tallman, K. A.; Lamberson, C. R.; Wang, X.; Hill, S.; Ivanova, P. T.; et al. Protein Modification by Endogenously Generated Lipid Electrophiles: Mitochondria as the Source and Target. *ACS Chem. Biol.* **2017**, *12*, 2062−2069.

(30) Alhouayek, M.; Bottemanne, P.; Makriyannis, A.; Muccioli, G. G. N-acylethanolamine-hydrolyzing acid amidase and fatty acid amide hydrolase inhibition differentially affect N-acylethanolamine levels and macrophage activation. *Biochim. Biophys. Acta Mol. Cell Biol. Lipids* **2017**, *1862*, 474−484.

(31) Ortega-Gutiérrez, S.; Molina-Holgado, E.; Guaza, C. Effect of anandamide uptake inhibition in the production of nitric oxide and in the release of cytokines in astrocyte cultures. *Glia* **2005**, *52*, 163−168.

(32) Molina-Holgado, F.; Molina-Holgado, E.; Guaza, C. The endogenous cannabinoid anandamide potentiates interleukin-6 production by astrocytes infected with Theiler's murine encephalomyelitis virus by a receptor-mediated pathway. *FEBS Lett.* **1998**, *433*, 139−142.

(33) Giordano, C.; Plastina, P.; Barone, I.; Catalano, S.; Bonofiglio, D. n-3 Polyunsaturated Fatty Acid Amides: New Avenues in the Prevention and Treatment of Breast Cancer. *Int. J. Mol. Sci.* **2020**, *21*, 2279.

(34) Thiele, C.; Papan, C.; Hoelper, D.; Kusserow, K.; Gaebler, A.; Schoene, M.; Piotrowitz, K.; Lohmann, D.; Spandl, J.; Stevanovic, A.; Shevchenko, A.; Kuerschner, L. Tracing Fatty Acid Metabolism by Click Chemistry. *ACS Chem. Biol.* **2012**, *7*, 2004−2011.

(35) Schwanhäusser, B.; Busse, D.; Li, N.; Dittmar, G.; Schuchhardt, J.; Wolf, J.; Chen, W.; Selbach, M. Global quantification of mammalian gene expression control. *Nature* **2011**, *473*, 337−342.

(36) Dandela, R.; Mantin, D.; Cravatt, B. F.; Rayo, J.; Meijler, M. M. Proteome-wide mapping of PQS-interacting proteins in Pseudomonas aeruginosa. *Chem. Sci.* **2018**, *9*, 2290−2294.

(37) Heo, S.; Kim, S.; Kang, D. The Role of Hydrogen Peroxide and Peroxiredoxins throughout the Cell Cycle. *Antioxidants* **2020**, *9*, 280.

(38) Knoops, B.; Argyropoulou, V.; Becker, S.; Ferté, L.; Kuznetsova, O. Multiple Roles of Peroxiredoxins in Inflammation. *Mol. Cells* **2016**, *39*, 60−64.

(39) Tae Lim, Y.; Sup Song, D.; Joon Won, T.; Lee, Y.-J.; Yoo, J.-S.; Eun Hyung, K.; Won Yoon, J.; Park, S.-Y.; Woo Hwang, K. Peroxiredoxin-1, a possible target in modulating inflammatory cytokine production in macrophage like cell line RAW264.7. *Microbiol. Immunol.* **2012**, *56*, 411−419.

(40) Phuyal, S.; Farhan, H. Multifaceted Rho GTPase Signaling at the Endomembranes. *Front. Cell Dev. Biol.* **2019**, *7*, 127.

(41) Wang, C.; Yoo, Y.; Fan, H.; Kim, E.; Guan, K.-L.; Guan, J.-L. Regulation of Integrin β1 Recycling to Lipid Rafts by Rab1a to Promote Cell Migration. *J. Biol. Chem.* **2010**, *285*, 29398−29405.

(42) Barbera, S.; Nardi, F.; Elia, I.; Realini, G.; Lugano, R.; Santucci, A.; Tosi, G. M.; Dimberg, A.; Galvagni, F.; Orlandini, M. The small GTPase Rab5c is a key regulator of trafficking of the CD93/Multimerin-2/β1 integrin complex in endothelial cell adhesion and migration. *Cell Commun. Signal.* **2019**, *17*, 55.

(43) Fowler, C. J. Transport of endocannabinoids across the plasma membrane and within the cell. *FASEB J.* **2013**, *280*, 1895−1904.

(44) McFarland, M. J.; Porter, A. C.; Rakhshan, F. R.; Rawat, D. S.; Gibbs, R. A.; Barker, E. L. A Role for Caveolae/Lipid Rafts in the Uptake and Recycling of the Endogenous Cannabinoid Anandamide. *J. Biol. Chem.* **2004**, *279*, 41991−41997.

(45) Brown, F. C.; Collett, M.; Tremblay, C. S.; Rank, G.; De Camilli, P.; Booth, C. J.; Bitoun, M.; Robinson, P. J.; Kile, B. T.; Jane, S. M.; et al. Loss of Dynamin 2 GTPase function results in microcytic anaemia. *Br. J. Haematol.* **2017**, *178*, 616−628.

(46) Marei, H.; Carpy, A.; Macek, B.; Malliri, A. Proteomic analysis of Rac1 signaling regulation by guanine nucleotide exchange factors. *Cell Cycle* **2016**, *15*, 1961−1974.

(47) Marei, H.; Carpy, A.; Woroniuk, A.; Vennin, C.; White, G.; Timpson, P.; Macek, B.; Malliri, A. Differential Rac1 signalling by guanine nucleotide exchange factors implicates FLII in regulating Rac1-driven cell migration. *Nat. Commun.* **2016**, *7*, 10664.

(48) Acevedo, A.; González-Billault, C. Crosstalk between Rac1-mediated actin regulation and ROS production. *Free Radic. Biol. Med.* **2018**, *116*, 101−113.

(49) Sadok, A.; Marshall, C. J. Rho GTPases. *Small GTPases* **2014**, *5*, No. e983878.

(50) Patel, R.; Attur, M. G.; Dave, M.; Abramson, S. B.; Amin, A. R. Regulation of Cytosolic COX-2 and Prostaglandin E2 Production by Nitric Oxide in Activated Murine Macrophages. *J. Immunol.* **1999**, *162*, 4191.